Desalination and Water Treatment
www.deswater.com
doi: 10.1080/19443994.2014.991945

57 (2016) 4523–4536
February

Taylor & Francis
Taylor & Francis Group

Effective removal of Cu^{2+} ions from aqueous solution in fixed-bed micro column using nanomagnetite-loaded poly (acrylamide-co-maleic acid) hydrogel as adsorbent

Neeraj Sharma, Alka Tiwari*

Department of Chemistry, Govt. V.Y.T. PG. Autonomous College, Durg 491001, Chhattisgarh, India, Tel. +09098190861; email: neeraj.sharma.shyam@gmail.com (N. Sharma), Tel. +07415514000; Fax: +07882324783; emails: brnsbarc18@gmail.com, alkatiwari18@yahoo.co.in (A. Tiwari)

Received 15 June 2014; Accepted 21 November 2014

ABSTRACT

The efficiency of nanomagnetite-loaded poly (acrylamide-co-maleic acid) hydrogel to remove Cu(II) ions from aqueous solution as well as contaminated water was studied in fixed-bed microcolumn. The effect of bed depth, inlet Cu(II) concentration and feed flow rate on the breakthrough characteristics of the adsorption system were determined in fixed-bed column studies. This study examined the applicability of the various empirical models to determine column dynamics by Thomas, Yoon–Nelson, and Adams–Bohart on copper ions removal from aqueous solution. The adsorbent has been found to be an efficient adsorbent for toxic Cu(II) ions from aqueous solution (>98% removal) and could be regenerated efficiently and used repeatedly for further experiments.

Keywords: Nanomagnetite; Adsorption; Fixed-bed column; Column dynamics; Copper ions

1. Introduction

Among various pollutants situated in surface and ground water, toxic heavy metal ions and their metalloids are of major concern as they are difficult to remove owing to their smaller ionic size, very low concentration in high volume, complex state of existence, nonbiodegradability, bioaccumulation in living tissues and competition with nontoxic inorganic species [1]. Copper and its compounds are ubiquitous in the environment and are thus found frequently in aqueous system. Industrial waste effluents from copper bearing acid mine drainage, metal cleaning, plating baths, metallurgical, pulp and paper, fertilizers, petroleum refining, wood preservation mining wastes discharge significant amount of dissolved copper in natural water resources and cause the contamination of water and soil due to copper as an toxin and carcinogen [2].

Copper behaves as toxin when reached beyond permissible limit ($1\,mg\,dm^{-3}$) in drinking water according to WHO. It is one of the most toxic ions to living organisms and prevails in the environment. Acute copper poisoning may cause systemic effects such as hemolysis liver and kidney damage and fever with influenza syndrome. Irritation of upper respiratory tract, epigastric burns, diarrhea, and gastrointestinal disturbance with vomiting, and a form of contact dermatitis are reported as local toxic effects of copper poisoning [3]. However, copper induced malformation of central nervous system of

*Corresponding author.

human fetuses has been reported [4]. Copper toxicity to living resources is essentially exerted on enzymes, particularly whose activities depends on amino and sulfhydryl groups because copper has high affinity for ligands containing nitrogen and sulfur donors [5]. Nucleic acids may also be the center of targets of toxic copper action [6].

Various processes exist for removing dissolved heavy metals from aqueous solution such as ion-exchange, reverse osmosis, adsorption, complexation and precipitation [7,8]. Many of these processes are not cost effective or difficult to implement in developing countries. Therefore, it is necessary to develop certain adequate treatment strategy that is simple, robust, and that addresses local resources and constraints. Sorption processes, including adsorption and ion-exchange, are a potential alternative for water and wastewater treatment. In recent years, considerable attention has been devoted to the study of removal of toxic metal ions from water by sorption using insoluble polymeric sorbents having different functional groups that can form complexes with metal cations from aqueous solutions [8,9]. Easy loading and in most cases, stripping of cations with simple chemicals, reusability, and the possibility of semicontinuous operation are the main advantages of such polymeric hydrogels [10]. A wide variety of polymeric sorbents having different functional groups were prepared and their complexing abilities were investigated [11–13].

This study examines the performance of nanomagnetite-loaded poly (acrylamide-co-maleic acid) hydrogel (nanomagnetite-loaded PAM hydrogel) for efficient removal of Cu(II) ions bearing aqueous solution as well as contaminated water in microcolumn sorption system. The efficiency of copper ions removal by the sorbent was studied as a function of different bed depth, flow rate, and inlet Cu(II) concentration in a fixed-bed column system. Column dynamics has been investigated by applying empirical models by Thomas, Yoon–Nelson, and Adams–Bohart for describing copper removal from aqueous solution on a fixed-bed of nanomagnetite-loaded PAM hydrogel.

For the purpose of comparison of adsorption capacity of PAM hydrogel with and without nanomagnetite impregnation, the column adsorption experiments were conducted. The PAM hydrogel loaded with nanomagnetite showed very high removal of Cu(II) ions (98%) whereas the adsorbent without nanomagnetite gave only 75.94% removal. Hence, encapsulation of nanomagnetite particles improved the efficiency of the novel adsorbent in the removal of Cu(II) ions from aqueous solution.

2. Material and methods

2.1. Materials

The monomers acrylamide and maleic acid were purchased from Loba Chemi, Mumbai and Himedia, Mumbai, India, respectively. N, N´-methylene-bis-acrylamide (cross-linker), potassium per sulfate (initiator), anhydrous ferric chloride, and ferrous chloride tetra hydrate were purchased from Molychem, Mumbai, India. Triple distilled water was used throughout the experiments.

2.2. Synthesis of nanomagnetite-loaded PAM hydrogel

To a mixture of acrylamide and maleic acid (1:1 ratio) the cross-linker (N, N´-methylene-bis-acrylamide) and initiator (potassium per sulfate) were added and heated at 70°C in an electric oven for 1 h. The copolymeric hydrogel so formed was washed with distilled water and cut into small uniform pieces. For *in situ* magnetization, these pieces were equilibrated in an aqueous solution of ferrous chloride and ferric chloride for 24 h. The Fe^{3+}-/Fe^{2+}-loaded pieces of copolymer were then added into conc. ammonia solution and kept overnight. The magnetic hydrogel was then washed thoroughly with distilled water, dried, and crushed into a fine powder.

2.3. Characterization of nanomagnetite-loaded PAM hydrogel

Nano magnetite loaded PAM hydrogel was characterized by TEM, AFM, SEM, FTIR, and XRD analysis.

2.3.1. TEM analysis

The average particle size, size distribution and morphology of ironoxide nanoparticles were examined using a TECNAI-G20 TEM at a voltage of 200 kV. The solvent dispersion of the particles was drop—cast onto a carboncoated copper grid and the grid was air dried at ambient conditions (25 ± 1°C) before loading into the microscope.

2.3.2. AFM analysis

The morphology and diameter of magnetite nanoparticles was examined by contact mode AFM (NS-E, Digital Instrument INC, USA) using silicon nitrate tip. The sample was prepared for AFM analysis by placing a few drops of the suspension of Fe_3O_4 in 50% HCl on a cleaved mica sheet (UGC-DAE, Indore, India).

2.3.3. SEM analysis

To examine the morphological characteristics of nanomagnetite-loaded PAM hydrogel before and after Cu(II) adsorption, samples were viewed using a scanning electron microscope (SAIF, Punjab University, Chandigarh).

2.3.4. XRD analysis

The crystalline nature of the bare nanomagnetite-loaded PAM hydrogel was studied on a Bruker D8 advanced X-ray Diffractometer with scanning range of 20°–80° (2θ) using Cu Kα radiation with wavelength of 1.5406 Å (UGC-DAE, Indore, India).

2.3.5. FTIR analysis

FTIR spectra of unabsorbed (bare) and Cu(II)-loaded adsorbent was recorded using varian vertex FTIR spectrometer (UGC-DAE, Indore, India).

2.4. Preparation of stock solution

Stock solution of Cu(II) of 1,000 mg dm^{-3} was prepared by dissolving 0.393 g $CuSO_4$ (AR) in 100 ml distilled water. Suitable concentrations of Cu(II) for column experiments were prepared by diluting the stock solution with distilled water.

2.5. Analytical techniques

The concentration of Cu(II) ions was determined using atomic absorption spectrometer (Varian AA-24-OFS model). Each experiment was carried out in triplicate under identical conditions to get the mean values.

2.6. Fixed-bed adsorption micro column study

Fixed-bed adsorption studies were conducted in a column made of polyethylene having an inner diameter of 0.5 cm and a height of 10 cm, at a constant temperature of 25°C. The column was packed with different bed heights of nanomagnetite-loaded PAM hydrogel on a glass–wool support. The experiments were performed at pH 6. The batch experimental results showed that the adsorption rate was high at pH 6 [14]. A known concentration of copper solution was allowed to pass through the bed at a constant flow rate (1 ml min^{-1}) in a down-flow manner. The copper solution was then collected at different time intervals until the column reached exhaustion and the concentration of Cu(II) ions was determined by atomic absorption spectrometer. The important design parameters such as column bed height, flow rate of metal solution into column and initial concentration of metal solution have been investigated.

2.7. Analysis of column data

The efficiency of the column was evaluated by determining breakthrough curves. The time for breakthrough appearance and the shape of the breakthrough curve are very important characteristics for determining the operation and the dynamic response of adsorption column. The breakthrough curves show the loading behavior of Cu(II) to be removed from solution in a fixed-bed and is usually expressed in terms of adsorbed metal concentration (C_{ad} = inlet metal concentration (C_0) − outlet metal concentration (C_t)) or normalized concentration defined as the ratio of effluent metal concentration to inlet metal concentration (C_t/C_0) as a function of time or volume of effluent for a given bed height [15]. The breakthrough time t_B is defined as the time required for the concentration of metal ions in the effluent to reach 5% of the applied concentration. The exhaustion time t_E is defined as the time when the concentration of metal ions in the effluent becomes 90% of the applied concentration. The breakthrough volumes V_B and exhaustion volumes V_E are the effluent volume at breakthrough time and exhaustion time, respectively. Effluent volume (V_{eff}) can be calculated from Eq. (1):

$$V_{eff} = Qt_{total} \tag{1}$$

where t_{total} and Q are the total flow time (min) and volumetric flow rate (ml min^{-1}), respectively. The area under the breakthrough curve (A) obtained by integrating the adsorbed concentration (C_{ad}; mg dm^{-3}) vs. t (min) plot can be used to find the total adsorbed metal quantity (maximum column capacity). Total adsorbed metal quantity (q_{total}; mg/g) in the column for a given feed concentration and flow rate (Q) is calculated from Eq. (2):

$$q_{total} = \frac{Q \cdot (C_0 - C_t) \cdot t_{total}}{1,000} \tag{2}$$

Total amount of metal ion sent to column (m_{total}) is calculated from Eq. (3):

$$m_{total} = \frac{C_0 \cdot Q \cdot t_{total}}{1,000} \tag{3}$$

Total removal percent of Cu(II) is the ratio of the maximum capacity of the column (q_{total}) to the total amount of Cu(II) sent to column (m_{total}) from Eq. (4):

$$\text{Total removal } (\%) = \frac{q_{total}}{m_{total}} \times 100 \tag{4}$$

Equilibrium metal uptake (q_{eq}) (or maximum capacity of the column) in the column is defined by Eq. (5) as the total amount of metal sorbed (q_{total}) per g of sorbent (X) at the end of the total flow time:

$$q_{eq} = \frac{q_{total}}{X} \tag{5}$$

2.8. Modeling of column dynamics

The sorption performance of the Cu(II) through the column was analyzed by BDST, Thomas, Yoon–Nelson, and Adams–Bohart models starting at concentration ratio, C_t/C_0 = breakthrough point until $C_t/C_0 > 0.90$ that is 90% breakthrough for copper by considering the safe water quality standards and operating limits of mass transfer zone of a column.

2.8.1. Bed depth service time model (BDST)

BDST is a simple model, which states that bed depth (Z) and service time (t) of a column bears a linear relationship. The linearized form of the model is given by Eq. (6):

$$t = \frac{N_0 Z}{C_0 Q} - \frac{1}{K_a C_0} \ln\left(\frac{C_0}{C_t} - 1\right) \tag{6}$$

where C_t is the breakthrough metal ion concentration (mg dm^{-3}), N_0 is the sorption capacity of bed (mg/L), Q is the flow rate (ml min^{-1}) and K_a is the rate constant (L/mg min).

2.8.2. Thomas model

The Thomas model is one of the most general and widely used models. The model is applicable in system with a constant flow rate and no axial dispersion, and its behavior matches the Langmuir isotherm and the second-order reversible reaction kinetics. The linearized form of the model is given by Eq. (7):

$$\ln\left(\frac{C_0}{C_t} - 1\right) = \frac{K_{Th} q_0 M}{Q} - \frac{K_{Th} C_0}{Q} V \tag{7}$$

In this expression K_{Th} (ml/mg min) is the Thomas rate constant, q_0 (mg/g) is the equilibrium adsorbate uptake, Q (ml/min) is the flow rate and V (ml) is the effluent volume. C_t is the concentration of metal ion at time t and C_0 is the initial metal ion concentration.

2.8.3. Yoon–Nelson model

A simple theoretical model developed by Yoon–Nelson was applied to investigate the breakthrough behavior of Cu(II) ions on nanomagnetite-loaded PAM hydrogel. This model is based on the assumption that the rate or decrease in the probability of adsorption for each adsorbate molecule is proportional to the probability of adsorbate adsorption and the probability of adsorbate breakthrough on the adsorbent. The Yoon–Nelson model is not only less complicated than other models but also requires no detailed data concerning the characteristics of adsorbate, the type of adsorbent and the physical properties of adsorption bed. The linearized model for a single component system is expressed by Eq. (8):

$$\ln\left(\frac{C_t}{C_0 - C_t}\right) = K_{YN} t - \tau \cdot K_{YN} \tag{8}$$

where K_{YN} (min^{-1}) is the Yoon–Nelson rate constant and τ is the time required for 50% adsorbate breakthrough (min), and t is the sampling time (min). C_t is the concentration of metal ion at time t and C_0 is the initial metal ion concentration.

For a given bed:

$$q_{0YN} = \frac{C_0 \cdot Q \cdot \tau}{1,000\ X} \tag{9}$$

where, q_{0YN} is the adsorption capacity, C_0 is the initial metal ion concentration, Q is the flow rate, X is the weight of adsorbent and τ is the 50% breakthrough time.

2.8.4. Adams–Bohart model

This model was established based on the surface reaction theory and it assumed that equilibrium is not instantaneous. Therefore the rate of adsorption was proportional to both the residual capacity of the adsorbent

and the concentration of the sorbing species. The mathematical equation of the model can be written as:

$$\ln\left(\frac{C_t}{C_0}\right) = K_{AB} \cdot C_0 \cdot t - K_{AB} \cdot q_{AB} \cdot \frac{Z}{Q} \quad (10)$$

where C_0 and C_t are the inlet and outlet adsorbate concentrations (mg dm^{-3}), respectively, K_{AB} is the rate constant (L/mg min), q_{AB} is the removal capacity (mg/L), Z (cm) is the bed depth, Q is the linear flow velocity (ml min^{-1}) and t is the service time (min).

Value of removal capacity q in mg/g is calculated as follows:

$$q = \frac{q_{AB} \cdot BV_s}{m} \quad (11)$$

where q is the removal capacity (mg/g), BV_s is the fixed-bed volume (L), and m is the mass of the bed (g).

2.9. Column desorption study

Column desorption study was carried out only after the column adsorption studies were conducted, at 25 ± 0.2°C, by using 0.1 M HNO_3 solution at flow rate of 1 ml min^{-1} and 1 cm bed depth to provide sufficient exchangeable H^+ ions for 240 min and then washed with hot distilled water and can be reused for further adsorption experiment.

3. Results and discussion

3.1. Characterization of nanomagnetite-loaded PAM hydrogel

The nano magnetite loaded PAM hydrogel was synthesized and characterized by the following instrumental methods.

3.1.1. TEM analysis

The shape, size, and morphology of ironoxide nanoparticles were determined through TEM imaging. The TEM images of nanoparticles show almost cubic-iron oxide particles with an average size of less than 10 nm, as shown in Fig. 1. Size of these nano particles lie within the range 1–9 nm. It should be noted, however, that the majority of the particles were scattered, few of them showing aggregates indicate stabilization of the nano particles. The results represented by TEM images concluded that the particle size of individual nanoparticles seem to be 1–10 nm, whereas majority of nanoparticles exhibit smaller sizes i.e. 5 and 8 nm.

3.1.2. AFM analysis

The morphology of the magnetite nanoparticles, using contact mode AFM, was found to be spherical, having size distribution in two different diameter (height) ranges of 10–20 nm (mean height: 15 nm) and 40–110 nm (mean height: 50 and 80 nm) as shown in Fig. 2. However, some larger particle size in figure may be a result of agglomeration of smaller magnetite nanoparticles in order to reduce the inherent large surface energies for magnetite nanoparticles.

3.1.3. SEM analysis

The SEM image of the sorbent surface is shown in Fig. 3 which clearly indicates the incorporation of nanomagnetite within copolymeric matrix. The surface appears quit heterogeneous and uneven. The presence of large voids make the surface quit heterogeneous and porous, which justify significant adsorption capacity of sorbent.

3.1.4. XRD analysis

The XRD pattern for the nanomagnetite-loaded PAM hydrogel is shown in Fig. 4. Five characteristic peaks ($2\theta = 30.09$, 35.44, 43.07, 56.96, and 62.55), marked by their indices [(511), (311), (400), (511), and (440)], were observed for nanomagnetite-loaded PAM hydrogel. The position and relative intensities of all diffraction peaks in Fig. 4 match well with those from the JCPDS file No. 89-5984 for magnetite (Fe_3O_4) and reveal that the prominent phase formed is Fe_3O_4 and the resultant nanoparticles of super paramagnetic ironoxide were pure magnetic with cubic structure.

Magnetite is obtained according to the reaction:

$$2FeCl_3 + FeCl_2 + 8NH_4OH \rightarrow Fe_3O_4 + 8NH_4Cl + 4H_2O$$

3.1.5. FTIR analysis

FTIR of bare and Cu(II)-adsorbed nanomagnetite-loaded PAM hydrogel are shown in Fig. 5(a) and (b) respectively. The FTIR analysis indicated the band at 2,930.55 cm^{-1}, assigned to C–H bond of methylene group. The FTIR analysis indicated the band due to acrylamide at 3,400, 1,640–1,650, 1,603, and 1,411 cm^{-1} attributed to N–H stretching, C=O stretching, N–H bending, and C–N stretching, respectively, which are

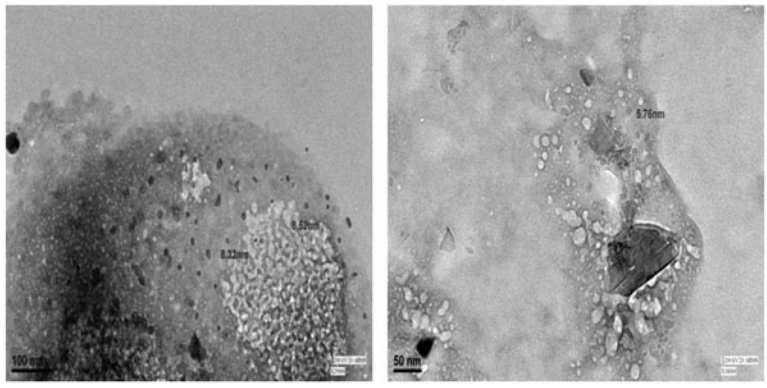

Fig. 1. Transmission electron micrograph of iron oxide nano particles.

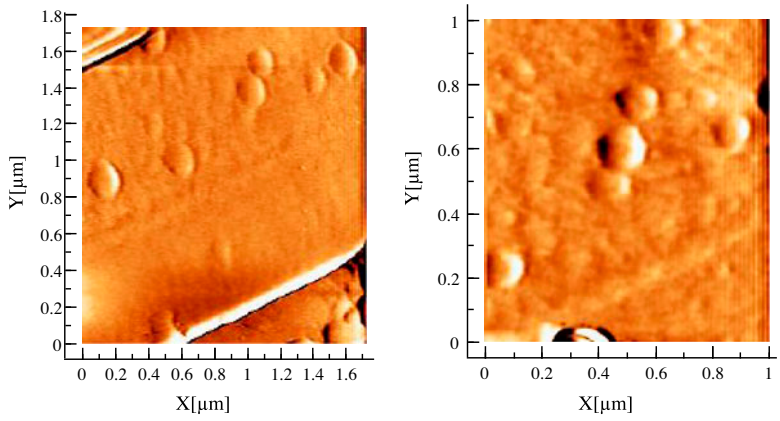

Fig. 2. AFM topographic images of magnetic nanoparticles on mica.

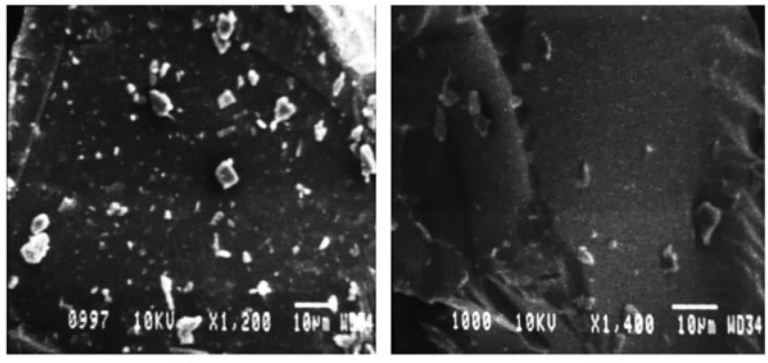

Fig. 3. SEM images of bare (a) nanomagnetite-loaded PAM hydrogel, (b) nanomagnetite-loaded PAM hydrogel after Cu(II) adsorption.

the characteristics of the amide ($CONH_2$) group. Absorption peaks due to maleic acid were also observed at 1,725 and 1,449 cm^{-1} for C=O and C–O stretching of the carboxylic (–COOH) group, respectively. The absorption peak at 3,446.24 cm^{-1} was assigned to –OH stretching, while a peak around 1,070.32 cm^{-1} may be due to the C–O stretching. The characteristic peak at 566.69 cm^{-1} relates to Fe–O

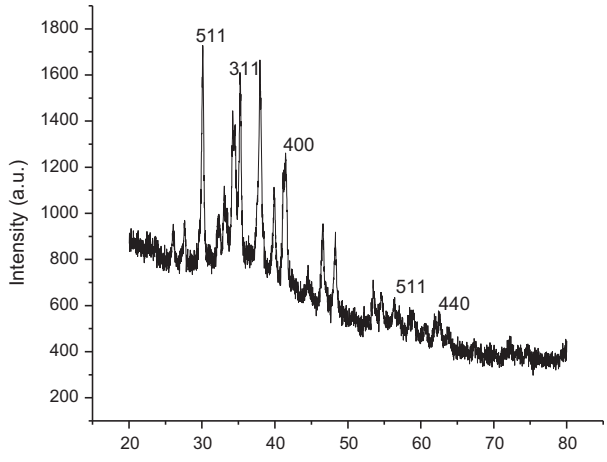

Fig. 4. XRD pattern of nanomagnetite-loaded PAM hydrogel.

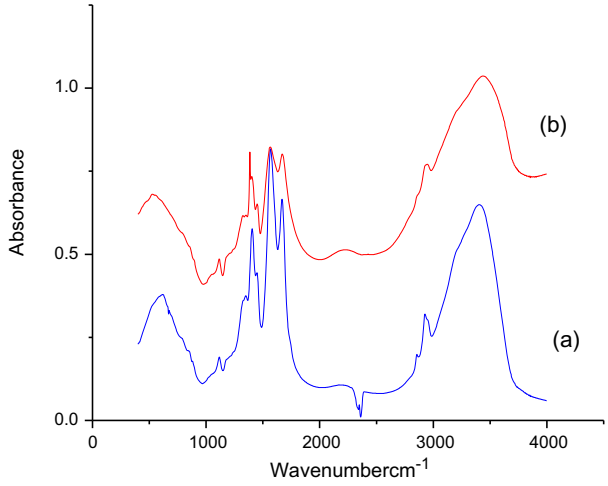

Fig. 5. FTIR pattern of (a) nano magnetite loaded PAM hydrogel before sorption of Cu(II) ions. (b) Nanomagnetite-loaded PAM hydrogel after sorption of Cu(II) ions.

group, which indicates the loading of nanoironoxide particles on PAM hydrogel because the surface of ironoxide with negative charges has an affinity toward PAM hydrogel, the magnetite nanoparticles could be loaded into protonated copolymer by the electrostatic interaction and chemical reaction through N,N´-methylene-bis-acrylamide cross linking. In Fig. 5(b) a slight change in shape and intensity of absorbance (due to $-CONH_2$ and –COOH groups) has been noticed. The change in the shape of the peak at 1,640–1,650 cm^{-1} (C=O stretching of primary amide groups in acrylamide units) and shifting of the peak (–NH stretching of amide groups) from 1,605 to 1,610 cm^{-1} may be arising due to the binding of primary amide group to Cu(II) ions with –COOH groups.

3.2. Mechanism of uptake

The nanomagnetite-loaded PAM hydrogel contains carboxyl and amide groups as confirmed by FTIR analysis, are responsible for binding the toxic Cu(II) ions on the surface. The proposed mechanism of binding the Cu(II) ions on various sites available at adsorbent surface (Fig. 6) may be explained as follows.

(1) Carboxylate groups ($-COO^-$) of maleic acid moiety of copolymer interact with Cu(II) ions.
(2) Cu(II) ions co-ordinate with the electron rich nitrogen of amide group of acrylamide moiety of copolymer.
(3) Cu(II) ions co-ordinate with the electron rich nitrogen of amide group of N, N´-methylene-bis-acrylamide moiety (cross-linking agent).
(4) In addition within the copolymer matrix, these Cu(II) ions may co-ordinate with the electron rich oxygen of magnetite nanoparticles.

3.3. Column studies of adsorption of Cu(II) ions onto nanomagnetite-loaded PAM hydrogel

Several operational factors such as bed depth (Z), flow rate (Q), and initial adsorbate concentration (C_0) affect the shape of a breakthrough curve and maximum capacity of the column. In this study, the effect of these parameters on breakthrough curve and maximum capacity of the column was investigated.

3.3.1. Effect of bed depth

The sorption breakthrough curves were obtained by varying bed depths ranging from 0.25 to 1 cm at 1 ml min^{-1} flow rate and 20 mg dm^{-3} initial copper ion concentrations, as shown in Fig. 7. It was observed that by increasing bed depth, there was an increase in bed capacity as well as in exhaustion time due to more binding sites were available for adsorption of copper ions. These results are also in agreement with those referred to the literature [16–19]. The values are given in Table 1.

3.3.2. Effect of flow rate

For investigating the influence of flow rate on the adsorption of Cu(II) ions, 20 mg dm^{-3} adsorbate solution was run through column of 1 cm bed depth by varying flow rate from 1 to 3 ml min^{-1}. Adsorption of metal ions was very rapid initially due to availability of binding sites for capturing metal ions around or

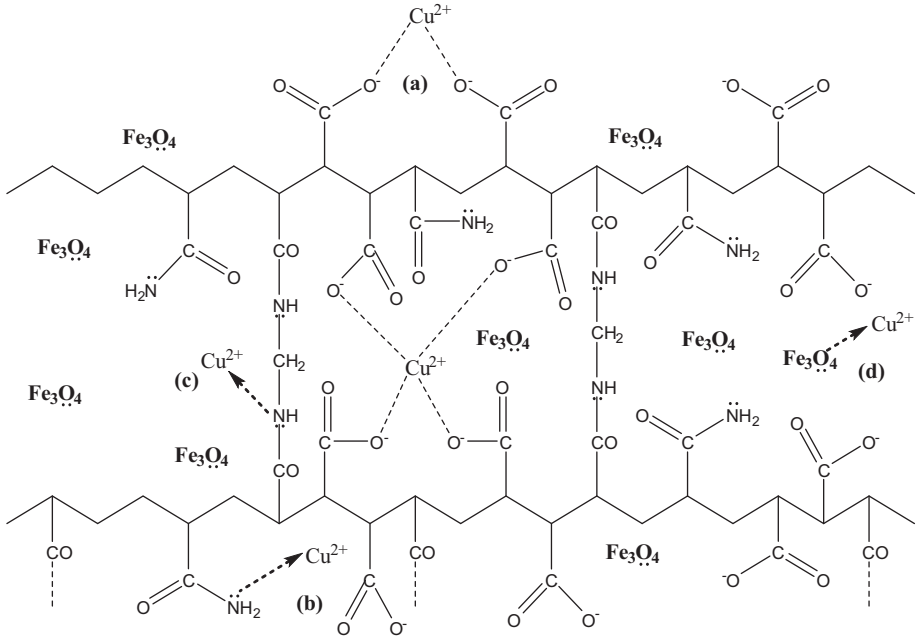

Fig. 6. Scheme of mechanism of Cu(II) ions uptake by nanomagnetite-loaded PAM hydrogel through co-ordination with (a) Carboxylate groups of maleic acid moiety, (b) electron rich nitrogen of amide group of acrylamide moiety, (c) electron rich nitrogen of amide group of N, N´-methylene-bis-acrylamide moiety (cross linking agent) (d) electron rich oxygen of magnetite nano particles.

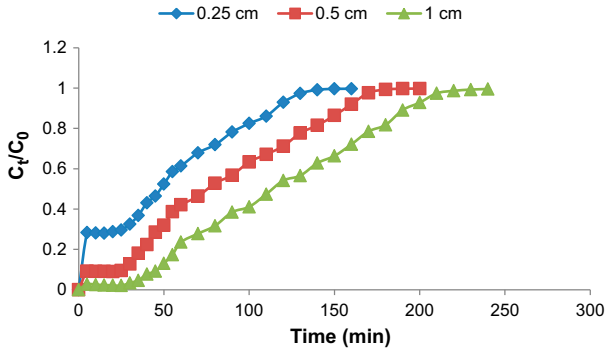

Fig. 7. The effect of bed depth on breakthrough curve at temperature = 25 ± 0.2°C, pH 6, bed depth of nanomagnetite-loaded PAM hydrogel = 0.25, 0.5, and 1 cm, flow rate = 1 ml min^{-1}, and Cu(II) initial concentration = 20 mg dm^{-1}.

inside the cells and then decreased due to gradual occupancy of these binding sites, hence uptake of metal ions becomes less effective and finally reached saturation. Fig. 8 shows that breakthrough curves become steeper and reach breakthrough quickly with increasing flow rate because contact time between copper ions and adsorbent is reduced at higher flow rates. Also at higher flow rate, the rate of mass transfer increased, thus the amount of Cu(II) adsorbed onto the unit bed height (mass transfer zone) increased as reported elsewhere [20,21]. The values are given in Table 2.

3.3.3. *Effect of initial copper ion concentrations*

It was observed that inlet metal ion concentration influenced the shape of breakthrough curves as shown

Table 1
The effect of bed depth on breakthrough curve at temperature = 25 ± 0.2°C, pH 6, bed depth of nanomagnetite-loaded PAM hydrogel = 0.25, 0.5, and 1 cm, and flow rate = 1 ml min^{-1}, and Cu(II) initial concentration = 20 mg dm^{-3}

Bed depth (cm)	Flow rate (ml min^{-1})	Inlet copper ion concentration (mg dm^{-3})	t_{total} (min)	m_{total} (mg)	q_{total} (mg)	q_{eq} (mg/g)	Removal (%)
0.25	1	20	160	3.2	2.302	23.02	71.94
0.5	1	20	200	4.0	3.641	18.205	91.03
1	1	20	240	4.8	4.701	11.753	97.94

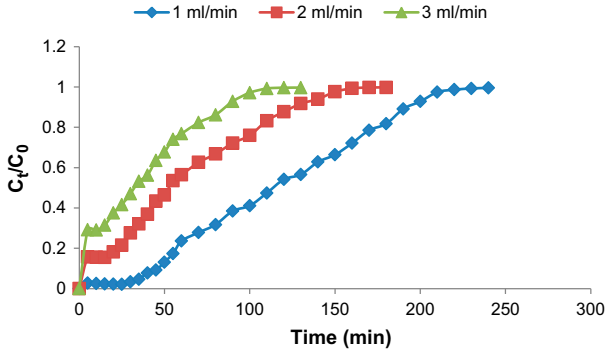

Fig. 8. The effect of flow rate on breakthrough curve at temperature = 25 ± 0.2°C, pH 6, flow rate = 1, 2, and 3 ml min^{-1}, bed height = 1 cm and Cu(II) initial concentration = 20 mg dm^{-3}.

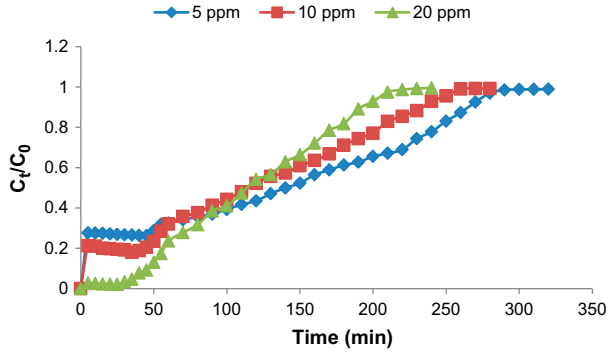

Fig. 9. The effect of inlet adsorbate concentration on breakthrough curve at temperature = 25 ± 0.2°C, pH 6, initial Cu(II) ion concentration = 5, 10, and 20 mg dm^{-3}, bed depth = 1 cm and flow rate = 1 ml min^{-1}.

in Fig. 9. With the increase in initial metal ion concentration, breakthrough curves become steeper. This is due to the increase in driving force and decrease in the adsorption zone length [22]. Similar trends have also been reported elsewhere [21,23]. At higher concentrations, available binding sites, situated on adsorbent surface, saturated more quickly resulted as early breakthrough time because of more adsorption sites being covered on increasing inlet metal ion concentration. Similar trend has also been observed for sorption of lead ions using granular slag column [24]. The values are given in Table 3.

3.4. Column kinetic study

The design and optimization of a fixed-bed sorption column need to employ some mathematical models, which must be used to describe and predict the experimental breakthrough curves, for possible scale up of process. The experimental adsorption data from the microcolumn studies was analyzed using BDST, Thomas, Yoon–Nelson, and Adams–Bohart models to analyze the column performance.

3.4.1. BDST model

The BDST model which is the plot of service time against bed depth at a flow rate of 1 ml min^{-1} was linear ($R^2 = 0.964$), thus indicating the validity of this model for the present system (shown in Fig. 10). The rate constant (K_a) and sorption capacity of bed (N_0) were calculated from the intercept and slope of BDST plot, respectively. The values of K_a and N_0 are given in Table 4. The rate constant K_a characterizes the rate of solute transfer from the fluid phase to the solid phase. If the value of K_a is high, then even a short bed will avoid breakthrough, but with low K_a value, a progressively longer bed will be required to avoid breakthrough [25]. The process parameter bed capacity (N_0) is used to predict the performance of the bed. As the bed depth increases, the residence time of the fluid inside the column increases, allowing the adsorbate molecules to diffuse deeper inside the adsorbent. Thus, the bed capacity will change with the change in service time [20].

Table 2
Results of breakthrough curve at different flow rates for adsorption of Cu(II) ions onto nanomagnetite-loaded PAM hydrogel at temperature = 25 ± 0.2°C, pH 6

Flow rate (ml min^{-1})	Bed depth (cm)	Inlet copper ion concentration (mg dm^{-3})	t_{total} (min)	m_{total} (mg)	q_{total} (mg)	q_{eq} (mg/g)	Removal (%)
1	1	20	240	4.8	4.701	11.753	97.94
2	1	20	180	7.2	6.084	15.21	84.50
3	1	20	130	7.8	5.536	13.84	70.97

Table 3
Results of breakthrough curve at different inlet adsorbate concentration for adsorption of Cu(II) ions onto nanomagnetite-loaded PAM hydrogel at temperature = 25 ± 0.2˚C, pH 6

Inlet copper ion concentration (mg dm^{-3})	Bed depth (cm)	Flow rate (ml min^{-1})	t_{total} (min)	m_{total} (mg)	q_{total} (mg)	q_{eq} (mg/g)	Removal (%)
5	1	1	320	1.6	1.180	2.950	73.75
10	1	1	280	2.8	2.296	5.740	82
20	1	1	240	4.8	4.701	11.753	97.94

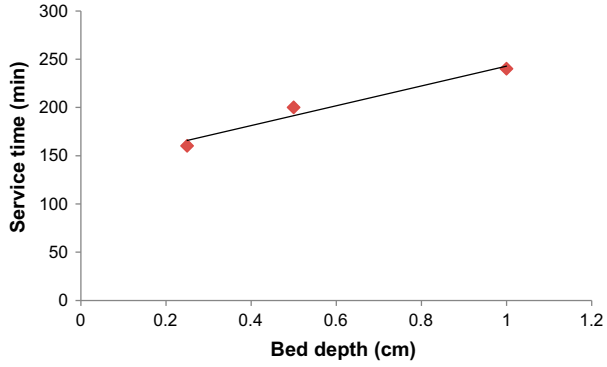

Fig. 10. BDST model of Cu(II) ions adsorption by nano-magnetite-loaded PAM hydrogel at temperature = 25 ± 0.2˚C, pH 6, flow rate = 1 ml min^{-1}, Cu(II) initial concentration = 20 mg dm^{-3}.

3.4.2. Thomas model

The experimental data were fitted with Thomas model to determine maximum capacity of sorption (q_0) and rate constant (K_{Th}). The K_{Th} and q_0 values were calculated from slope and intercept of linear plots of ln $[(C_0/C_t) - 1]$ against t at different flow rates, bed heights, and initial metal ion concentration using values from the column experiments (Figures are not shown). It can be concluded on the basis of the regression coefficient (R^2) and other parameters that the experimental data fitted well with Thomas model. The model parameters are listed in Table 5. As the concentration increased, the value of K_{Th} decreased whereas the value of q_0 showed a reverse trend, i.e. increased with increase in concentration. The maximum bed capacity (q_0) decreased with increase in flow rate as well as bed depth. K_{Th} values increased with increase in the flow rate but decreased with increase in the bed depth. Similar trends have also been observed for sorption of Cr(VI) using activated weed fixed bed-column [26] and removal of Pb(II) onto granular activated carbon derived from *Mangostana garcinia* shell [27]. The experimental data fitted well with the Thomas model.

3.4.3. Yoon–Nelson model

A plot of ln $[C_e/(C_0 - C_e)]$ vs. t gave a straight line with slope of K_{YN} and intercept of $-\tau \cdot K_{YN}$. The values of K_{YN}, τ, and adsorption capacity q_0 are listed in Table 6. The results show that K_{YN} increased with the increase in concentration, whereas the 50% breakthrough time, τ decreased. This may be due to the fact that the increase in initial copper ion concentration increases the competition between adsorbate molecules for the adsorption site, which ultimately results in the increased uptake rate [28]. These results are also in agreement with the results obtained by Nwabanne and Igbokwe [29]. Also, the adsorption capacity q_0 increased with increase in initial copper ion concentration and decreased with increase in bed depth and flow rate. The rate constant increased with the increase in flow rate but decreased with the increase in bed depth. The time required for 50% breakthrough τ decreased with increase in flow rate and increased with increase in bed depth. High values of correlation coefficients indicate that Yoon–Nelson model fitted well to the experimental data. This is in agreement with the results obtained by Tsai et al. [30]. For this model, the calculated tau values are quite close to

Table 4
Calculated constant of bed depth service time equation for adsorption of Cu(II) ions onto nanomagnetite-loaded PAM hydrogel

Adsorbent	N_0 (mg/L)	K_a (L/mg/min)	R^2
Nano magnetite loaded PAM hydrogel	2,056	0.0014	0.964

Table 5
Thomas model parameters of adsorption of Cu (II) ions onto nanomagnetite-loaded PAM hydrogel at different conditions using linear regression analysis

S. No.	Factors	Thomas model parameters		
		K_{Th} (ml/min/mg)	q_0 (mg/g)	R^2
1.	Bed height (cm)			
(a)	0.25	1.65	9.830	0.988
(b)	0.5	1.45	8.379	0.964
(c)	1	1.45	5.969	0.959
2.	Flow rate (ml min^{-1})			
(a)	1	1.45	5.969	0.959
(b)	2	3.2	2.961	0.983
(c)	3	6.3	1.652	0.994
3.	Initial Cu(II) concentration (mg dm^{-3})			
(a)	5	2.4	1.743	0.935
(b)	10	1.6	3.084	0.976
(c)	20	1.45	5.969	0.959

Table 6
Yoon–Nelson model parameters of adsorption of Cu(II) ions onto nanomagnetite-loaded PAM hydrogel at different conditions using linear regression analysis

S. No.	Factors	Yoon–Nelson model parameters			
		K_{YN} (min^{-1})	τ (min)	q_0 (mg/g)	R^2
1.	Bed height (cm)				
(a)	0.25	0.033	49.18	9.836	0.992
(b)	0.5	0.029	83.76	8.376	0.969
(c)	1	0.029	119.66	5.983	0.958
2.	Flow rate (ml min^{-1})				
(a)	1	0.029	119.66	5.983	0.958
(b)	2	0.032	59.22	5.922	0.983
(c)	3	0.042	33.05	4.958	0.994
3.	Initial Cu(II) concentration (mg dm^{-3})				
(a)	5	0.012	139.42	1.743	0.935
(b)	10	0.016	123.31	3.083	0.976
(c)	20	0.029	119.66	5.983	0.958

those found experimentally, which indicates that the parameters of the model are similar to those obtained in the experiments.

3.4.4. Adams–Bohart model

Linear plots of ln (C_t/C_0) against time, t at different bed depths, initial metal ion concentrations and flow rates were plotted (Figures are not shown). Values of K_{AB} and q_{AB} were calculated from the slope and intercept of the linear curves, respectively, and listed in Table 7. Values of K_{AB} increased with increase in bed depth but decreased with increase in flow rate and initial metal ion concentration. However, q_{AB} values decreased for increasing bed depth but increased for increasing flow rate and initial metal ion concentration. Poor correlation coefficients indicate less applicability of this model [31].

3.5. Desorption studies

Desorption results indicated 99.89% recovery of Cu(II) ions from the surface of the sorbent using 0.1 M HNO_3 in 5 h at 25°C temperature, the results are shown in Fig. 11. The nanomagnetite-loaded PAM hydrogel showed almost the same metal ion

Table 7
Adams–Bohart model parameters of adsorption of Cu(II) ions onto nanomagnetite-loaded PAM hydrogel at different conditions using linear regression analysis

S. No.	Factors	Adams-Bohart model parameters			
		K_{AB} (L/mg min)	q_{AB} (mg/L)	q (mg/g)	R^2
1.	Bed height (cm)				
(a)	0.25	0.6	9.067	14.507	0.916
(b)	0.5	0.7	5.8	5.8	0.828
(c)	1	0.8	3.594	2.156	0.813
2.	Flow rate (ml min^{-1})				
(a)	1	0.8	3.594	2.156	0.813
(b)	2	0.65	4.895	2.203	0.864
(c)	3	0.7	5.096	1.656	0.916
3.	Initial Cu (II) concentration (mg dm^{-3})				
(a)	5	1	1.425	1.14	0.993
(b)	10	0.7	2.344	1.641	0.928
(c)	20	0.8	3.594	2.156	0.813

adsorption capacity after the repeated regeneration. It may be stated that, in acidic medium, protons compete with Cu(II) ions and displace the maximum amount of adsorbed copper. Hence, ion-exchange mechanism is important in connection with adsorption–desorption process for adsorbent.

3.6. Treatment of industrial effluent

The efficiency of the nanomagnetite-loaded PAM hydrogels for the removal of toxic copper ions was tested with a metal polishing industrial wastewater sample. The optimum conditions for removal of copper ions by nanomagnetite-loaded PAM hydrogel in a column system has already described in experimental part. The amount of copper ions present in sample (before and after adsorption) was determined by atomic absorption spectrometer. Initially the concentration of copper ion was found to be 18.8174 mg dm^{-3} in effluent water. The breakthrough curve of column study is shown in Fig. 12. The results were in good agreement with those obtained from column experiments conducted for copper ions removal in synthetic wastewater samples. 98.42% removal of copper was obtained in column adsorption study.

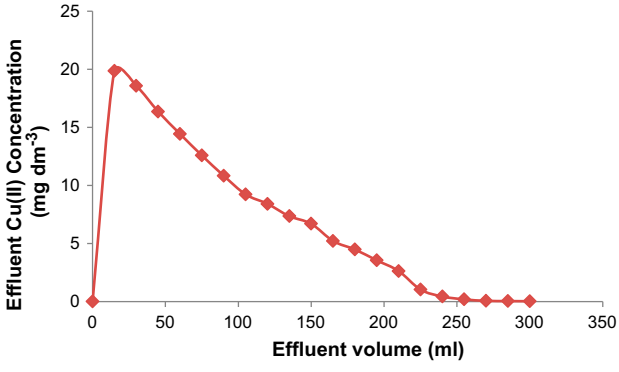

Fig. 11. Desorption studies of Cu(II) ions using 0.1 M HNO_3 solution with Cu(II) adsorbed fixed-bed microcolumn of nanomagnetite-loaded PAM hydrogel at temperature = 25 ± 0.2 ℃, flow rate = 1 ml min^{-1}, and bed depth = 1 cm.

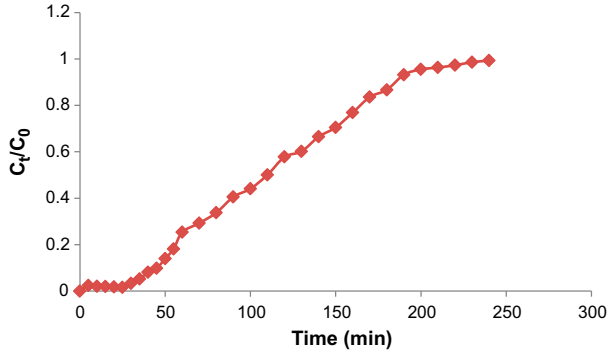

Fig. 12. Breakthrough curve for adsorption of copper onto nanomagnetite-loaded poly (acrylamide-co-maleic acid) hydrogel at bed height = 1 cm, flow rate = 1 ml min^{-1}, pH 6, temperature = 25 ± 0.2 ℃.

4. Conclusion

The adsorbent "nanomagnetite-loaded PAM hydrogel" has been found to be an effective, efficient, and

inexpensive adsorbent for Cu (II) removal from aqueous solution as well as effluent water. The effects of bed depth, inlet feed concentration, and flow rate on Cu(II) ion adsorption were investigated and experimental breakthrough curves were obtained. The experiments were performed at 1 ml min^{-1} flow rate, 1 cm bed depth, and 20 mg dm^{-3} inlet copper ion concentration at pH 6. It was observed that equilibrium metal uptake (q_0) increased with increase in flow rate and inlet copper ion concentration and decreased with increase in bed depth. Both breakthrough point and exhaustion time increased with increase in bed depth and inlet copper ion concentration and decreased with increase in flow rate. Thomas, Yoon–Nelson, and Adams-Bohart kinetic models were used to describe the column adsorption kinetics. The experimental breakthrough curve was compared satisfactorily with the breakthrough profile calculated by Thomas and Yoon–Nelson method. The calculated column parameters could be scaled up for the design of fixed-bed columns for effective and efficient removal of toxic metal ions from water.

Acknowledgements

The authors would like to express thanks to the Department of Atomic Energy, BRNS-BARC, Mumbai, India for providing financial assistance. Authors are also grateful to UGC-DAE Consortium for Scientific Research, Indore for FTIR and AFM analysis and AIIMS, New Delhi, India for TEM analysis.

References

[1] I.A. Abideen, E.O. Andrew, A.I. Mopelola, S. Kareem, Equilibrium, kinetics and thermodynamic studies of the biosorption of Mn(II) ions from aqueous solution by raw and acid-treated corn cob biomass, Res. J. Appl. Sci. 6 (2011) 302–309.

[2] A.K. Meena, G.K. Mishra, P.K. Rai, C. Rajagopal, P.N. Nagar, Removal of heavy metal ions from aqueous solutions using carbon aerogel as an adsorbent, J. Hazard. Mater. 122 (2005) 161–170.

[3] S. Rengaraj, Y. Kim, C.K. Joo, J. Yi, Removal of copper from aqueous solution by aminated and protonated mesoporous aluminas: Kinetics and equilibrium, J. colloid. Interface Sci. 273 (2004) 14–21.

[4] J. Aaseth, T. Norseth, Handbook on the Toxicity of Metals, Elsevier, Amsterdam, 1986, pp. 233–257.

[5] C.A. Flemming, J.T. Trevors, Copper toxicity and chemistry in the environment: A review, Water Air Soil Pollut. 44 (1989) 143–158.

[6] G. Tyler, M.B. Pahlsson, G. Bengtsson, E. Baath, L. Tranvik, Heavy metal ecology of terrestrial plants, microorganisms and invertebrates, Water Air Soil Pollut. 47 (1989) 189–215.

[7] E. Erdem, N. Karapinar, R. Donat, The removal of heavy metal cations by natural zeolites, J. Colloid. Interface Sci. 280 (2004) 309–314.

[8] W.S. Wan Ngah, C.S. Endud, R. Mayanar, Removal of copper (II) ions from aqueous solution onto chitosan and cross-linked chitosan beads, React. Funct. Polym. 50 (2002) 181–190.

[9] B. George, V.N.R. Rajasekharan Pillai, B. Mathew, Effect of the nature of the crosslinking agent on the metal-ion complexation characteristics of 4 mol % DVB- and NNMBA-crosslinked polyacrylamide-supported glycines, J. Appl. Polym. Sci. 74 (1999) 3432–3444.

[10] H. Kaşgöz, A. Kaşgöz, Ü. Şahin, T.Y. Temelli, C. Bayat, Hydrogels with acid groups for removal of copper (II) and lead (II) ions, Polym. Plast. Technol. Eng. 45 (2006) 117–124.

[11] H. Kaşgöz, S. Özgümüş, M. Orbay, Preparation of modified polyacrylamide hydrogels and application in removal of Cu(II) ion, Polymer 42 (2001) 7497–7502.

[12] H. Kaşgöz, S. Özgümüş, M. Orbay, Modified polyacrylamide hydrogels and their application in removal of heavy metal ions, Polymer 44 (2003) 1785–1793.

[13] B.L. Rivas, G.V. Seguel, K.E. Geckeler, Synthesis, characterization, and properties of polychelates of poly (styrene sulfonic acid-co-maleic acid) with Co(II), Cu(II), Ni(II), and Zn(II), J. Appl. Polym. Sci. 85 (2002) 2546–2551.

[14] A. Tiwari, N. Sharma, Efficiency of superparamagnetic nano iron oxide loaded poly (acrylamide-co-maleic acid) hydrogel in uptaking Cu^{2+} ions from water, J. Dispersion Sci. Technol. 34 (2013) 1437–1446.

[15] Z. Aksu, F. Gönen, Biosorption of phenol by immobilized activated sludge in a continuous packed bed: Prediction of breakthrough curves, Process Biochem. 39 (2004) 599–613.

[16] Z. Zulfadhly, M.D. Mashitah, S. Bhatia, Heavy metals removal in fixed-bed column by the macro fungus *Pycnoporus sanguineus*, Environ. Pollut. 112 (2001) 463–470.

[17] J.T. Nwabanne, P.K. Igbokwe, Adsorption performance of packed bed column for the removal of lead (II) using oil palm fibre, Int. J. Appl. Sci. Technol. 2(5) (2012) 106–115.

[18] E. Malkoc, Y. Nuhoglu, Removal of Ni(II) ions from aqueous solutions using waste of tea factory: Adsorption on a fixed-bed column, J. Hazard. Mater. 135 (2006) 328–336.

[19] E. Malkoc, Y. Nuhoglu, Fixed bed studies for the sorption of chromium (VI) onto tea factory waste, Chem. Eng. Sci. 61 (2006) 4363–4372.

[20] D.C.K. Ko, J.F. Porter, G. McKay, Optimised correlations for the fixed-bed adsorption of metal ions on bone char, Chem. Eng. Sci. 55 (2000) 5819–5829.

[21] V.C. Taty-Costodes, H. Fauduet, C. Porte, Y.S. Ho, Removal of lead (II) ions from synthetic and real effluents using immobilized *Pinus sylvestris* sawdust: Adsorption on a fixed-bed column, J. Hazard. Mater. 123 (2005) 135–144.

[22] J. Goel, K. Kadirvelu, C. Rajagopal, V.K. Kumar Garg, Removal of lead (II) by adsorption using treated granular activated carbon: Batch and column studies, J. Hazard. Mater. 125 (2005) 211–220.

[23] K. Vijayaraghavan, J. Jegan, K. Palanivelu, M. Velan, Removal of nickel (II) ions from aqueous solution using crab shell particles in a packed bed up-flow column, J. Hazard. Mater. 113 (2004) 223–230.
[24] S.V. Dimitrova, Use of granular slag columns for lead removal, Water Res. 36 (2002) 4001–4008.
[25] K. Vijayaraghavan, J. Jegan, K. Palanivelu, M. Velan, Batch and column removal of copper from aqueous solution using a brown marine alga *Turbinaria ornata*, Chem. Eng. J. 106 (2005) 177–184.
[26] S.S. Baral, N. Das, T.S. Ramulu, S.K. Sahoo, S.N. Das, G.R. Chaudhury, Removal of Cr(VI) by thermally activated weed Salvinia cucullata in a fixed bed column, J. Hazard. Mater. 161 (2009) 1427–1435.
[27] Z.Z. Chowdhury, S.M. Zain, R.A. Khan, R.F. Rafique, K. Khalid, Batch and fixed adsorption studies of lead (II) cations from aqueous solutions onto granular activated carbon derived from Mangostana garcinia shell, Bioresources 7(3) (2012) 2895–2915.
[28] P. Sivakumar, P.N. Palanisamy, Adsorption studies of basic Red 29 by a non-conventional activated carbon prepared from Euphorbia antiquorum L, Int. J. Chem. Tech. Res. 1(3) (2009) 502–510.
[29] J.T. Nwabanne, P.K. Igbokwe, Kinetic modeling of heavy metals adsorption on fixed bed column, Int. J. Environ. Res. 6(4) (2012) 945–952.
[30] W.T. Tsai, C.Y. Chang, C.Y. Ho, L.Y. Chen, Simplified description of adsorption breakthrough curves of 1,1-dichloro-1-fluoroethane (HCFC-141b) on activated carbon with temperature effect, J. Colloid. Interface Sci. 214 (1999) 455–458.
[31] G.S. Bohart, E.Q. Adams, Some aspects of the behavior of charcoal with respect to chlorine, J. Am. Chem. Soc. 42(3) (1920) 523–544.